15th IAPR International Conference on Machine Vision Applications (MVA)
Nagoya University, Nagoya, Japan, May 8-12, 2017.

Design and Analysis of a Novel Omnidirectional Stereovision System

Lei Luo
Department of Information Science and Electronic Engineering
Zhejiang University, Hangzhou, China
luolei@zju.edu.cn

Zhiyu Xiang
Zhejiang Provincial Key Laboratory of Information and Network
Zhejiang University, Hangzhou, China
xiangzy@zju.edu.cn

Abstract

Omnidirectional stereovision has wide applications in object detection, three-dimensional reconstruction and robot navigation thanks to its large field-of-view. In this paper, a novel configuration that consists of one single camera and multiple mirrors is proposed. The significant improvement is to design a principal mirror above the four sub mirrors placed in a plane to achieve four pairs of stereovision. A projection model with configuration parameters of this system is investigated in order to analyze the precision in reconstruction. Furthermore, the error propagation from image points to the triangulated 3D points and the effects of the system parameters on resulting measurement error are also given. Based on the simulation results, the optimal interval of these parameters is obtained.

1 Introduction

Unlike the perspective camera that can only provide a narrow conic section of view, the omnidirectional catadioptric vision system makes it possible for a camera to capture nearly half-sphere of the surrounding environment at once. Thanks to its wide filed-of-view, there is an increase popularity in the development of omnidirectional vision for extensive applications such as motion estimation [1], object detection [2], SLAM [3], surveillance [4] and robot navigation [5]. To realize an omnidirectional stereo vision system, the widely used technique is to combine a single camera with multiple convex mirrors so that the object can be reflected in several mirror surfaces to recover the depth. Moreover, instead of moving or rotating the camera to take photos around, the catadioptric omnidirectional vision system is able to produce a panorama in one single step without image stitch.

In the past decades, various configurations of omnidirectional stereo-vision system have been proposed. According to the arrangement of the mirrors, the system structures can be divided into two categories: 1) mirrors are vertically coaxial; 2) mirrors are placed on a horizontal plane. For the first category, initial work in this field was probably published by Southwell et al. [6], in which a special shaped, double-lobed mirror was implemented. However, due to the small baseline, it's hard to obtain high precision. Later in [7], five different physical configurations that possess two vertically aligned mirrors were thoroughly analyzed and compared. Although the number of mirrors was limited, they employed an approximated technique that could simulate the shape of spherical, parabolic and equiangular mirrors. In addition, since equiangular mirrors have a linear relationship between the angle changed in incident rays and that changed in refection rays, Lui [5] and Sturzl [8] explored further researches with this type of mirror. Especially in [5], an automatic baseline selection algorithm was described in order to determine a suitable vertical-baseline for the current environment. Apart from the equiangular mirror, Labutov at el. [9] designed a catadioptric rig composed of two coaxially-aligned spherical mirrors of different radii. An intriguing utilization in [9] was the fusion of depth given by optical flow and stereoscopy. Unfortunately, computing dense optical flow could not achieve real-time performance.

As for the second category, Sagawa [2] created an omnidirectional sensor that had a large, spherical mirror with seven small mirrors around. This sensor is light and portable, but its accuracy in stereovision might not be achieved for the reason that the sub mirrors are too small to capture high-quality image for reconstruction. In [10], the authors placed four parabolic mirrors in a square at the same distance from the camera for the purpose of pose estimation and robot self-localization. To deal with various types of mirrors, Xiang et al. [11] developed a sub-camera array model with off-center spherical projection for catadioptric multi-mirror system. Despite that plenty of omnidirectional systems have been applied in computer vision, it is still hard to evaluate between them, let alone making an optimal choice. To figure out this question, Mouaddib et al. [12] proposed several criteria including useful image surface, reconstruction accuracy and view field to make comparisons between these configurations. This work did go a step further in the second category, while vertical aligned mirrors were not taken into discussion. In particular, Dequen et al. [13] provided a local search technique to find the best parameters in system design, but it is under the assumption that mirrors can't overlap each other.

The configuration proposed in this paper literally integrates the properties in both categories mentioned above. It consists of one principal mirror, four sub mirrors and a camera with a telecentric lens. The four sub mirrors are symmetrically located in a horizontal plane. Taking the sub mirrors as a union, the relative pose between the principal mirror and this union can be regarded as a vertical alignment. In this way, the baseline contains the horizontal and the vertical part, which is much longer than any part alone to guarantee the precision. The compact system structure is also benefit for mobility.

This paper is organized as follows. Section 1 gives a brief overview of related works. Section 2 describes the proposed omnidirectional stereovision system in detail.

The error analysis and simulation results of the system parameters are presented in Section 3. Section 4 summarizes the whole paper.

2 System Structure and Imaging Model

The system consists of one principal mirror with four sub mirrors and a single camera equipped with a telecentric lens that effectively integrates stereovision and omnidirectional vision together. Sub mirrors are placed in a plane perpendicular to the optical axis while the principal mirror is above them and its focus is on the optical axis.

A standard configuration of the system is illustrated in Fig.1. From the viewpoint of the camera, the system structure is rotationally symmetrical and the center of each sub mirror is on the edge of the principal mirror to make high utilization in image and less occlusion in stereovision simultaneously. Parabolic mirror is selected for the orthographic projection because of its good performance in misalignment cases. All these mirrors have the uniform size and curvature so that they possess the same angle of view to assure the 3D reconstruction between every two adjacent mirrors.

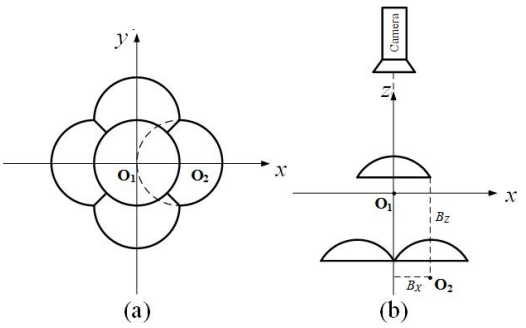

Figure 1. A standard system configuration. (a)Top view (b)Side View

Since the visual system is perfectly symmetrical, to analyze a pair of mirrors that contains the principal mirror and one sub mirror is enough. As shown in Fig.2, the point O_1 is the focus of the principal paraboloid while the point O_2 is the focus of the sub paraboloid. Taking the reference frame at O_1-xyz, the relative pose between two paraboloids can be denoted by $T = [B_X, 0, -B_Z]^T$.

Given a 3D world point $P(X, Y, Z)$, it is projected to the focus O_1 to obtain the intersection point Q_1 on the principal mirror surface. With orthographic projection, Q_1 is mapped to the virtual normalized image plane as $(x_1, y_1, 1)$ and the pixel point is obtained by

$$\begin{pmatrix} u_1 \\ v_1 \\ 1 \end{pmatrix} = \begin{pmatrix} f_x & 0 & u_0 \\ 0 & f_y & v_0 \\ 0 & 0 & 1 \end{pmatrix} \begin{pmatrix} x_1 \\ y_1 \\ 1 \end{pmatrix} \tag{1}$$

where f_x, f_y and u_0, v_0 are the intrinsic parameters of the orthographic camera.

Similarly, the point $P(X, Y, Z)$ can be projected to the focus O_2 to get an intersection point Q_2, and the corresponding point in the normalized image plane is $(x_2, y_2, 1)$.

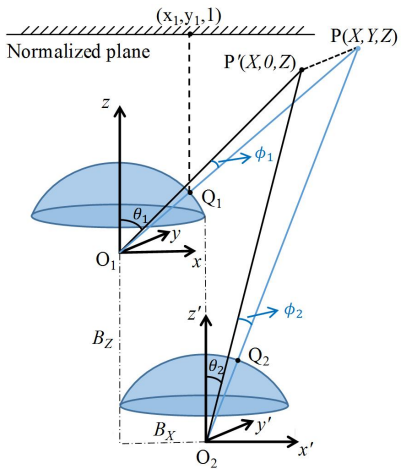

Figure 2. The projection model

In order to analyze the relationship between the 3D spatial points and the image points, a vertical projection angle ϕ and a horizontal projection angle θ is defined, as illustrated in Fig.2. ϕ_1 represents the projection angle between O_1P and xO_1z plane while θ_1 denotes the angle between O_1P' and z-axis, where P' is the vertical projection of 3D point P in xO_1z plane.

Define the two paraboloid functions as $x^2 + y^2 = -4p(z - p)$ and $(x - B_X)^2 + y^2 = -4p(z - B_Z - p)$. The 3D coordinates of the object point P can be reconstructed by Eq.(2).

$$\begin{cases} X = Z\tan\theta_1 = \frac{(B_Z\tan\theta_2 + B_X)\tan\theta_1}{\tan\theta_1 - \tan\theta_2} \\ Y = \frac{Z\tan\phi_1}{\cos\theta_1} = \frac{(Z+B_Z)\tan\phi_2}{\cos\theta_2} \\ Z = \frac{B_Z\tan\theta_2 + B_X}{\tan\theta_1 - \tan\theta_2} \end{cases} \tag{2}$$

where $\tan\theta_1 = \frac{4px_1}{4p^2-(x_1^2+y_1^2)}$, $\frac{\tan\phi_1}{\cos\theta_1} = \frac{4py_1}{4p^2-(x_1^2+y_1^2)}$, $\tan\theta_2 = \frac{4p(x_2-B_X)}{4p^2-[(x_2-B_X)^2+y_2^2]}$, $\frac{\tan\phi_2}{\cos\theta_2} = \frac{4py_2}{4p^2-[(x_2-B_X)^2+y_2^2]}$, respectively.

At this point the relationship between the world coordinates $P(X, Y, Z)$ and the image coordinates $(x_1, y_1), (x_2, y_2)$ has been obtained. The reconstruction error analysis can then be derived from it.

3 Error Analysis and Simulation

3.1 Reconstruction error analysis

The Eq.(2) can be rewritten as,

$$P(X, Y, Z) = f(p, B_X, B_Z, x_1, x_2, y_1, y_2) \tag{3}$$

where p, B_X, B_Z are the system parameters in this model, x_1, x_2, y_1, y_2 are the coordinates in the normalized image plane, respectively.

The total error of a 3D point is generally represented by the partial error on X, Y and Z, that is

$$\begin{aligned} \Delta e_{\text{total}} &= \sqrt{\Delta X^2 + \Delta Y^2 + \Delta Z^2} \\ &= \sqrt{\sum_m \sum_{X,Y,Z} \left(\frac{\partial P(X,Y,Z)}{\partial m} \cdot \delta_m \right)^2} \end{aligned} \tag{4}$$

where m denotes each parameter in Eq.(3), and δ_m represents the measuring error of each parameter.

Thus, combining Eq.(4) with Eq.(2), the error propagation function can be expressed as follows.

$$\begin{cases} \frac{\partial X}{\partial x_1} = -\frac{(B_X \tan\theta_2 + B_X)\tan\theta_2}{(\tan\theta_1 - \tan\theta_2)^2} \cdot \frac{\partial \tan\theta_1}{\partial x_1} \\ \frac{\partial X}{\partial y_1} = -\frac{(B_Z \tan\theta_2 + B_X)\tan\theta_2}{(\tan\theta_1 - \tan\theta_2)^2} \cdot \frac{\partial \tan\theta_1}{\partial y_1} \\ \frac{\partial X}{\partial x_2} = \frac{(B_Z \tan\theta_1 + B_X)\tan\theta_1}{(\tan\theta_1 - \tan\theta_2)^2} \cdot \frac{\partial \tan\theta_2}{\partial x_2} \\ \frac{\partial X}{\partial y_2} = \frac{(B_Z \tan\theta_1 + B_X)\tan\theta_1}{(\tan\theta_1 - \tan\theta_2)^2} \cdot \frac{\partial \tan\theta_2}{\partial y_2} \end{cases} \tag{5}$$

$$\begin{cases} \frac{\partial Z}{\partial x_1} = -\frac{B_Z \tan\theta_2 + B_X}{(\tan\theta_1 - \tan\theta_2)^2} \cdot \frac{\partial \tan\theta_1}{\partial x_1} \\ \frac{\partial Z}{\partial y_1} = -\frac{B_Z \tan\theta_2 + B_X}{(\tan\theta_1 - \tan\theta_2)^2} \cdot \frac{\partial \tan\theta_1}{\partial y_1} \\ \frac{\partial Z}{\partial x_2} = \frac{B_Z \tan\theta_1 + B_X}{(\tan\theta_1 - \tan\theta_2)^2} \cdot \frac{\partial \tan\theta_2}{\partial x_2} \\ \frac{\partial Z}{\partial y_2} = \frac{B_Z \tan\theta_1 + B_X}{(\tan\theta_1 - \tan\theta_2)^2} \cdot \frac{\partial \tan\theta_2}{\partial y_2} \end{cases} \tag{6}$$

$$\begin{cases} \frac{\partial Y}{\partial x_1} = \frac{\partial Z}{\partial x_1} \cdot \frac{\tan\phi_1}{\cos\theta_1} + \frac{\partial(\frac{\tan\phi_1}{\cos\theta_1})}{\partial x_1} \cdot Z \\ \frac{\partial Y}{\partial y_1} = \frac{\partial Z}{\partial y_1} \cdot \frac{\tan\phi_1}{\cos\theta_1} + \frac{\partial(\frac{\tan\phi_1}{\cos\theta_1})}{\partial y_1} \cdot Z \\ \frac{\partial Y}{\partial x_2} = \frac{\partial (Z+B_X)}{\partial x_2} \cdot \frac{\tan\phi_2}{\cos\theta_2} + \frac{\partial(\frac{\tan\phi_2}{\cos\theta_2})}{\partial x_2} \cdot (Z+B_Z) \\ \frac{\partial Y}{\partial y_2} = \frac{\partial (Z+B_X)}{\partial y_2} \cdot \frac{\tan\phi_2}{\cos\theta_2} + \frac{\partial(\frac{\tan\phi_2}{\cos\theta_2})}{\partial y_2} \cdot (Z+B_Z) \end{cases} \tag{7}$$

where $\frac{\partial \tan\theta_1}{\partial x_1} = \frac{4p(4p^2+x_1^2-y_1^2)}{(4p^2-x_1^2-y_1^2)^2}$, $\frac{\partial \tan\theta_1}{\partial y_1} = \frac{8px_1y_1}{(4p^2-x_1^2-y_1^2)^2}$, $\frac{\partial \tan\theta_2}{\partial x_2} = \frac{4p[4p^2+(x_2-B_X)^2-y_2^2]}{[4p^2-(x_2-B_X)^2-y_2^2]^2}$, $\frac{\partial \tan\theta_2}{\partial y_2} = \frac{8p(x_2-B_X)y_2}{[4p^2-(x_2-B_X)^2-y_2^2]^2}$, $\frac{\partial(\frac{\tan\phi_1}{\cos\theta_1})}{\partial x_1} = \frac{2x_1}{(4p^2-x_1^2-y_1^2)^2}$, $\frac{\partial(\frac{\tan\phi_1}{\cos\theta_1})}{\partial y_1} = \frac{4p(4p^2-x_1^2+y_1^2)}{(4p^2-x_1^2-y_1^2)^2}$, $\frac{\partial(\frac{\tan\phi_2}{\cos\theta_2})}{\partial x_2} = \frac{2(x_2-B_X)}{[4p^2-(x_2-B_X)^2-y_2^2]^2}$, $\frac{\partial(\frac{\tan\phi_2}{\cos\theta_2})}{\partial y_2} = \frac{4p[4p^2-(x_2-B_X)^2+y_2^2]}{[4p^2-(x_2-B_X)^2-y_2^2]^2}$, respectively.

3.2 Error distribution map

In the following experiments, we set $B_X = 3.0$ cm, $B_Z = 10.5$ cm, $r = 3.0$ cm and $p = 3.0$, where r denotes the radius of mirrors. Take a 3D world point $P(X, Y, Z)$ in the plane with $Z = 100$ cm, $X \in [1, 150]$ cm and $Y \in [-150, 150]$ cm are reconstructed, which almost covers the mutual visual field of the pair of mirrors.

With the 3D point $P(X, Y, Z)$ and the projection model, corresponding image coordinates (x_1, y_1) and (x_2, y_2) can be computed easily. In order to simplify the calculation, suppose the measure error in the normalized image plane is $\delta_{x_1} = \delta_{x_2} = \delta_{y_1} = \delta_{y_2} = \delta = 0.005$. Then, using Eq.(4-7), the total error distribution map in three-dimensional space is achieved (Fig.3).

The error distribution map is symmetrical about the straight line $Y = 0$ and possesses a valley point at about $P(65, 0, 100)$ with minimum reconstruction error. Meanwhile, it indicates that the central region, which is marked by dark blue, keeps relative small error. When the 3D point P moves away from the center, the total error gradually goes up along with the increase in distance. To make a clearer illustration for the distribution of accuracy in image plane, the error is mapped back to the normalized image plane (Fig.4), in which the deeper the color, the smaller the error. Thus, the dark blue region represents the optimal range for stereovision and 3D reconstruction.

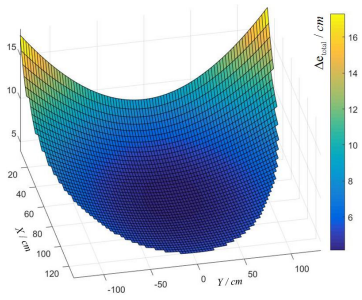

Figure 3. The distribution of the reconstruction error in three-dimensional space.

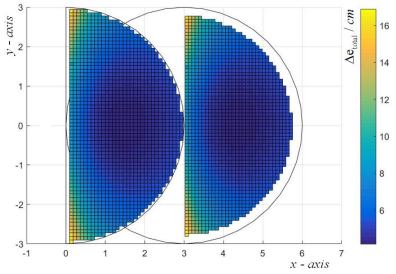

Figure 4. The error distribution map in the normalized image plane.

3.3 Simulation on the optimal system parameters

Based on the experiments in section 3.2, the position $P(65, 0, 100)$ with minimum error is used for further simulations to search optimal system parameters B_X, B_Z and p.

The results on the total error when P is set at different distances are compared in Fig.5(a), in which B_Z varies in [1,30]. The three curves have the same trend that the error falls quickly at first and then tend to be stable. Taking both small error and appropriate relative pose into consideration, a value between [10,20] for B_Z will be a good choice.

Similarly, simulations of B_X are carried out and their performances are depicted in Fig.5(b), which again proves that the error and B_X are inversely related. As B_X varies from 1 cm to 6 cm, the center of sub mirror gradually moves away from the principal mirror. Generally, a short B_X causes more severe occlusion in sub mirror, while a longer B_X brings about larger blank region in image plane. Only with more useful area in image that contains information reflected by the mirrors can we assure the accuracy for stereovision. Thus, take into account all the factors mentioned above, the optimal value of B_X should be close to or a little greater than the mirror radius. And here in this case, the best interval for B_X is [2.5,4].

Fig.5(c) illustrates the change of reconstruction error relative to the mirror parameter p. The curves initially falls, and then levels off when p is greater than 2.5. The zeros in Fig.5(c) indicate that the 3D point P is out of view. It is worth noting that when the radius r is fixed, the variation of p significantly affects the field of view. As for a paraboloid, the field of view decreases rapidly

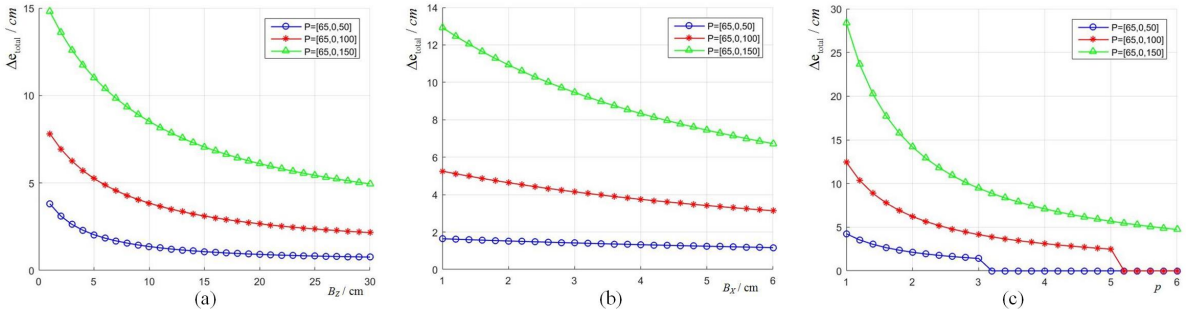

Figure 5. (a)The error distribution curve of $B_Z \in [1, 30]$ cm. (b)The error distribution curve of $B_X \in [1, 6]$ cm. (c)The error distribution curve of $p \in [1, 6]$.

with the increase of p. Although the greater p results in smaller error, it also leads to narrower field of view. Hence, to balance the situation, it is recommended that determining the view angle first and then adjusting the radius r and the factor p to the requirement.

4 Conclusion

A novel multi-mirror omnidirectional stereovision system and its projection model are proposed in this paper. The system is composed of one principal mirror with four sub mirror and a camera with telecentric lens to achieve wide field-of-view, so that adequate information reflected by every two adjacent mirrors can be used for stereo reconstruction. With projection model, the error propagation from image points to the corresponding triangulation points is probed, based on which the error distribution map is obtained. Furthermore, the effects of all these system parameters on measurement error are analyzed separately. Based on the simulation results, reasonable value intervals for each of the parameters are attained. Our future work will focus on building a real system based on the proposed scheme and further verifying the effectiveness of the system.

Acknowledgements

This work was sponsored by National Natural Science Foundation of China under grant No. 61571390, Zhejiang Provincial Natural Science Foundation under grant No. LY15F010004, and Fundamental Research Funds for the Central Universities. The Authors would like to express sincere appreciation for their support.

References

[1] V.-D. Hoang, D. C. Hernández, D. Seo, and K.-H. Jo, "Optimal angular back-projection error for vehicle motion estimation using omnidirectional vision," in *2014 IEEE/ASME International Conference on Advanced Intelligent Mechatronics*, pp. 658–663, IEEE, 2014.

[2] R. Sagawa, N. Kurita, T. Echigo, and Y. Yagi, "Compound catadioptric stereo sensor for omnidirectional object detection," in *Intelligent Robots and Systems, 2004.(IROS 2004). Proceedings. 2004 IEEE/RSJ International Conference on*, vol. 3, pp. 2612–2617, IEEE, 2004.

[3] H. Erturk, G. Tuna, T. V. Mumcu, and K. Gulez, "A performance analysis of omnidirectional vision based simultaneous localization and mapping," in *International Conference on Intelligent Computing*, pp. 407–414, Springer, 2012.

[4] M. Findeisen, L. Meinel, M. Heß, A. Apitzsch, and G. Hirtz, "A fast approach for omnidirectional surveillance with multiple virtual perspective views," in *EUROCON, 2013 IEEE*, pp. 1578–1585, IEEE, 2013.

[5] W. L. D. Lui and R. Jarvis, "Eye-full tower: A gpu-based variable multibaseline omnidirectional stereovision system with automatic baseline selection for outdoor mobile robot navigation," *Robotics and Autonomous Systems*, vol. 58, no. 6, pp. 747–761, 2010.

[6] D. Southwell, A. Basu, M. Fiala, and J. Reyda, "Panoramic stereo," in *Pattern Recognition, 1996., Proceedings of the 13th International Conference on*, vol. 1, pp. 378–382, IEEE, 1996.

[7] M. Ollis, H. Herman, and S. Singh, *Analysis and design of panoramic stereo vision using equi-angular pixel cameras*. Carnegie Mellon University, The Robotics Institute, 1999.

[8] W. Stürzl, H. jürgen Dahmen, and H. A. Mallot, "The quality of catadioptric imaging–application to omnidirectional stereo," in *European Conference on Computer Vision*, pp. 614–627, Springer, 2004.

[9] I. Labutov, C. Jaramillo, and J. Xiao, "Generating near-spherical range panoramas by fusing optical flow and stereo from a single-camera folded catadioptric rig," *Machine vision and applications*, vol. 24, no. 1, pp. 133–144, 2013.

[10] G. Caron, E. Marchand, and E. M. Mouaddib, "3d model based pose estimation for omnidirectional stereovision," in *2009 IEEE/RSJ International Conference on Intelligent Robots and Systems*, pp. 5228–5233, IEEE, 2009.

[11] Z. Xiang, Y. Zhou, and X. Gong, "A novel sub-camera array model for calibrating multi-mirror catadioptric systems," *Measurement Science and Technology*, vol. 26, no. 8, p. 085402, 2015.

[12] E. M. Mouaddib, R. Sagawa, T. Echigo, and Y. Yagi, "Stereovision with a single camera and multiple mirrors," in *Proceedings of the 2005 IEEE International Conference on Robotics and Automation*, pp. 800–805, IEEE, 2005.

[13] G. Dequen, L. Devendeville, and E. Mouaddib, "Stochastic local search for omnidirectional catadioptric stereovision design," in *Iberian Conference on Pattern Recognition and Image Analysis*, pp. 404–411, Springer, 2007.